ADVANCED PHOTONICS RESEARCH
Open Access
www.adpr-journal.com

Theoretical and Experimental Evidence of Two-Step Tautomerization in Hypericin

Quan Liu, Liangxuan Wang, Juan Carlos Roldao, Pierre-Michel Adam, Marc Brecht, Johannes Gierschner, Frank Wackenhut,* and Alfred J. Meixner**

Hypericin has large potential in modern medicine and exhibits fascinating structural dynamics, such as multiple conformations and tautomerization. However, it is difficult to study individual conformers/tautomers, as they cannot be isolated due to the similarity of their chemical and physical properties. An approach to overcome this difficulty is to combine single molecule experiments with theoretical studies. Time-dependent density functional theory (TD-DFT) calculations reveal that tautomerization of hypericin occurs via a two-step proton transfer with an energy barrier of 1.63 eV, whereas a direct single-step pathway has a large activation energy barrier of 2.42 eV. Tautomerization in hypericin is accompanied by reorientation of the transition dipole moment, which can be directly observed by fluorescence intensity fluctuations. Quantitative tautomerization residence times can be obtained from the autocorrelation of the temporal emission behavior revealing that hypericin stays in the same tautomeric state for several seconds, which can be influenced by the embedding matrix. Furthermore, replacing hydrogen with deuterium further proves that the underlying process is based on tunneling of a proton. In addition, the tautomerization rate can be influenced by a $\lambda/2$ Fabry–Pérot microcavity, where the occupation of Raman active vibrations can alter the tunneling rate.

1. Introduction

Tautomerization is a fundamental process in nature[1,2] and binding affinities of a molecule to a protein/receptor depend on its tautomeric state,[3–5] which is crucial for, e.g., drug design.[6] In addition, tautomerization can influence chemical reactivity.[7–9] A well-explored example is the proton transfer of porphyrins[10–12] and porphycenes,[13–16] where tautomerization occurs by tunneling of the two protons in the framework of the four inner nitrogen atoms. However, even these structurally similar molecules exhibit different tautomerization mechanisms with a step wise process in porphyrin[11,17] and a concerted mechanism including vibrational activation in porphycenes.[13] Hence, it is essential to have an as detailed as possible understanding of the underlying processes. However, a major challenge to study tautomerization is that individual tautomeric species often cannot be isolated[9] and single-molecule spectroscopy and theoretical studies are used to overcome this difficulty. Single-molecule spectroscopy/microscopy has the major advantage that it avoids ensemble averaging and hence allows to observe processes, such as diffusion,[18] spectral diffusion,[19,20] or intramolecular proton transfer,[21] which are hidden in a classical ensemble experiment. Similarly, single-molecule experiments enable to study conformational transitions and tautomerization of hypericin, a molecule which can be found

Q. Liu, L. Wang, Prof. M. Brecht, Dr. J. Gierschner, Dr. F. Wackenhut, Prof. A. J. Meixner
Institute of Physical and Theoretical Chemistry
Eberhard Karls University Tübingen
Auf der Morgenstelle 18, Tübingen 72076, Germany
E-mail: johannes.gierschner@imdea.org; frank.wackenhut@uni-tuebingen.de; alfred.meixner@uni-tuebingen.de

Q. Liu, Prof. P.-M. Adam
Laboratoire Lumière nanomatériaux & nanotechnologies – L2n and CNRS ERL 7004
Universitéde Technologie de Troyes
Troyes 10000, France

Prof. M. Brecht
Process Analysis and Technology (PA&T)
Reutlingen Research Institute
Reutlingen University
Alteburgstraße 150, Reutlingen 72762, Germany

L. Wang, J. C. Roldao, Dr. J. Gierschner
Madrid Institute for Advanced Studies
IMDEA Nanoscience
Ciudad Universitaria de Cantoblanco
C/Faraday 9, Madrid 28049, Spain

The ORCID identification number(s) for the author(s) of this article can be found under https://doi.org/10.1002/adpr.202000170.

© 2021 The Authors. Advanced Photonics Research published by Wiley-VCH GmbH. This is an open access article under the terms of the Creative Commons Attribution License, which permits use, distribution and reproduction in any medium, provided the original work is properly cited.

DOI: 10.1002/adpr.202000170

in nature in *Hypericum perforatum* (St. John's wort). Hypericin has been used as folk medicine throughout history and is a promising natural drug due to its antidepressive, antineoplastic, antitumor, and antiviral activity. Especially, its application in photodynamic therapy has drawn considerable attention,[22–24] as it is the strongest natural photo sensitizer and allows to visualize tumor cells by its red fluorescence emission.[25] However, hypericin is not only of medical interest, but is also a fascinating molecule to study fundamental physical/chemical processes, as it can undergo excited and ground-state tautomerization, de-/protonation, and conformational transitions.[26–33] Indeed, many ensemble studies are dealing with the optical properties of hypericin, covering fluorescence[34] and phosphorescence emission,[35,36] fluorescence lifetime,[37] Raman and SERS spectrum.[38–40] Despite its large triplet yield, hypericin is well suited for single molecule experiments allowing to investigate phenomena usually averaged in an ensemble.[41,42] But, the complex photo physics are a blessing and a curse, as it is difficult to pin down the origin of a specific change. However, time-dependent density functional theory (TD-DFT) offers a solid theoretical framework to correlate with the experimental data and permits to calculate isomer energies,[43] transition states,[44] and the transition dipole moment (TDM).[45]

TD-DFT calculations of hypericin show that the TDM of its tautomers differs in strength and orientation,[42] which opens up the possibility to study individual tautomers by optical microscopy. Here, we use confocal microscopy combined with higher-order laser modes, namely azimuthally polarized doughnut mode (APDM) and radially polarized doughnut mode (RPDM).[46–48] These modes are especially interesting for single-molecule studies, as they allow to excite all molecules regardless of their 3D orientation and to directly observe the orientation of the TDM by the orientation and shape of the image pattern.[49,50] In particular, the orientation of the TDM in the sample plane can be monitored by the APDM due to its exclusively transversal electric field distribution, whereas the RPDM allows to determine the full 3D orientation of the TDM.[51,52] This technique enables to directly observe the reorientation of the TDM caused by tautomerization via the flipping of the image pattern.[21,53] In the study by Liu et al.,[42] we have shown that the individual tautomers of hypericin can be identified and studied on the single-molecule level by this technique. Here, we show that tautomerization of hypericin can additionally be observed in the temporal fluorescence emission behavior and quantitative results can be obtained from the intensity autocorrelation function. This allows to study how the tautomerization rate is influenced by the matrix in which the molecule is embedded or by exchanging the tunneling proton with deuterium. Furthermore, we study hypericin embedded in an optical photonic $\lambda/2$ microcavity consisting of two semitransparent silver mirrors supporting resonances in the visible spectral range. The optical mode density in such a microcavity can enhance/suppress the spontaneous emission rate by the Purcell effect[54] and allows to tune the fluorescence lifetime and enhance specific transitions of a molecule or nanoparticle without altering its structure.[55–58] In addition, the occupation of Raman active vibrations can be amplified,[59–62] which leads to an influence of the photonic environment on the tautomerization rate.

2. Results and Discussion

Typical fluorescence images of single hypericin molecules acquired with the APDM and RPDM are shown in **Figure 1**.

The APDM is exclusively polarized in the image plane and the orientation of the double lobe image pattern is given by the in-plane orientation of the TDM, which is indicated by the double arrows in Figure 1a. On the contrary, the RPDM is primarily polarized perpendicular to the image plane, i.e., parallel to the optical axis, when focused with a high numerical aperture (NA) objective lens. This field distribution of the excitation focus enables to determine the full 3D orientation of a single molecule.[21,49–51] The shapes of RPDM image patterns reveals that molecules 1 and 2 are nearly parallel to the image plane resulting in symmetric double lobe patterns in Figure 1b. The RPDM pattern shapes of molecules 3 and 4 in Figure 1b are asymmetric, hence they are tilted out of the image plane with an angle of 47° and 38°, respectively. However, the RPDM has the drawback of a weaker in-plane component and molecule 5 is not visible in Figure 1b. Imaging with the APDM/RPDM has the advantage, that processes involving a reorientation of the TDM, such as tautomerization, can be directly observed by flipping of the image pattern.[21,42,63] Apart from the spatial TDM orientation, also information about the temporal emission behavior is contained in the microscopy images. The acquisition time of a single image is around 60 s with 5 ms integration time per pixel. Hence, molecules 3 and 4 show a reorientation of the TDM on the seconds time scale and alternating dark and bright pixels of the image patterns of molecule 5 indicate milliseconds dynamics without reorientation of the TDM, since such a fast reorientation of the TDM would result in a ring like pattern shape. However, hypericin exhibits a rather complex photophysical behavior, as it can undergo excited and ground state tautomerization,

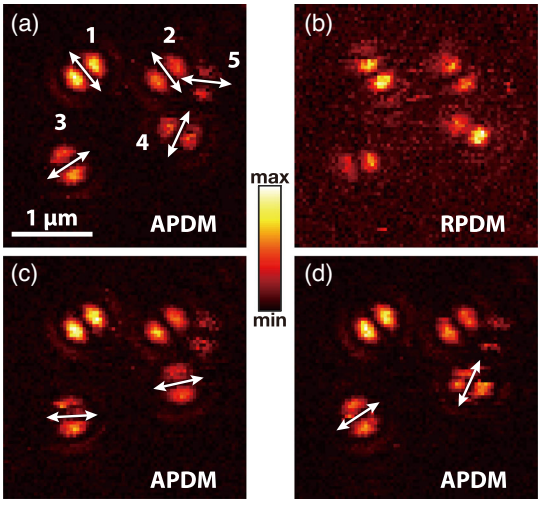

Figure 1. a) Series of successive fluorescence images recorded at the same spatial position over 4 min. Scanning range is 3×3 µm^2 (75 pixels $\times$ 75 pixels, 5 ms per pixel). a,c,d) are excited with the APDM and b) is excited with the RPDM. Five single hypericin molecules labeled 1–5 can be observed and the in-plane orientation of their TDM is indicated by the white arrows. Molecules 3 and 4 show a flipping of their image pattern in successive images due to tautomerization.

© 2021 The Authors. Advanced Photonics Research published by Wiley-VCH GmbH

de-/protonation, conformational (torsional) transitions, as well as possible association (dimerization).[26] Hence, it is, without further knowledge, difficult to pin down the origin of the dynamics shown in Figure 1. TD-DFT simulations are an appropriate tool to get further insights into these complex dynamics and results obtained for different hypericin conformations are shown in **Figure 2**.

Hypericin offers a rich structural variety of conformational and positional isomers due to the presence of six hydroxyl and two keto groups, as well as methyl groups in the bay region of the naphthodianthrone core.[26] In fact, the methyl-substitutions at the bay region contribute to a distorted aromatic parent backbone.[27] Four different conformers can be achieved by torsions of the skeleton and the substitutes, namely, the "propeller" form (^{P}M-Q, ^{P}P-Q) and the "butterfly" form (^{B}M-Q, ^{B}P-Q),[27] as shown in Figure 2. As discussed earlier,[26,27,64] conformers ^{P}M-Q/^{P}P-Q (^{B}M-Q/^{B}P-Q) are isoenergetic, enantiomeric pairs, distinguished by the reflection symmetry, whereas ^{P}M-Q/^{B}M-Q (^{P}P-Q/^{B}P-Q) are diastereomers. Conformational isomerization proceeds via transition states ^{1}T and ^{2}T, see Figure 2a. This was shown earlier by force field (FF) calculations,[27] and was recalculated here at the DFT level to obtain more reliable values, especially for the transition states. The Gibbs free energy of ^{B}M-Q is by 8.7 kJ mol^{-1} (0.09 eV) less stable than ^{P}M-Q, see Figure 2b and Figure S1, Supporting Information, which is significantly more than the FF results.[27] The energy barriers corresponding to the deformation at the hydroxyl and the methyl half plane were estimated to be $E(^{1}\mathrm{T}) = 246$ kJ mol^{-1} (2.55 eV) and $E(^{2}\mathrm{T}) = 333$ kJ mol^{-1} (3.45 eV), respectively, being again much higher than the FF results.[27] For ^{2}T, an extra distortion resulting from the steric requirements of two adjacent methyl substitutes is responsible for the higher energy barrier.

Apart from the torsional isomerization, we identify a second conformational coordinate, being a H-flipping at the hydroxyl groups, see Figure 2b. Here, two hydrogen atoms alternatively participate in the formation of the intramolecular hydrogen bond, i.e., hydrogen bonds pointing upward or downward. Due to the fact that hypericin belongs to the point group of C_2, proton transfer in this bond shifting process leads to an identical species. The energy barriers in this coordinate amounted to be 145 (1.50) and 239 kJ mol^{-1} (2.48 eV) for ^{P}M-Q and ^{B}M-Q, respectively.

In a second step, transition states for tautomerization were investigated. We exemplify here on the most probable intramolecular one-proton-transfer between the most stable $Q_{7,14}$ and $Q_{1,7}$ tautomers; for the nomenclature, see **Figure 3**, for a comprehensive scheme see, Figure S2, Supporting Information, and for a classification of the different tautomers, see previous studies for reference.[27,42] Starting from $Q_{7,14}$, there are two possible pathways to reach $Q_{1,7}$. In the single-step pathway (dashed arrow in Figure 3), a pronounced geometrical distortion occurs at the position 14 (TS_1); here, the significant torsion leads to a high energy barrier of 233 kJ mol^{-1} (2.42 eV), see Figure 3b. In the two-step path (solid arrows in Figure 3), $Q_{7,14}$ will first cross an intermediate state $Q_{7,14\text{-}M^*}$ (energy difference: 140 kJ mol^{-1} [1.45 eV]) via the proton transfer at the position 13, then reach $Q_{1,7}$ via a second proton transfer at the position 14. The transition states (TS_2 and TS_3) in the second pathway induces slight distortions, consequently reflecting lower energy barriers with $E(TS_2) = 154$ kJ mol^{-1} (1.60 eV) and $E(TS_3) = 157$ kJ mol^{-1} (1.63 eV), which is thus energetically favored, and suggested as the pathway observed in the experiments. Replacing the responsible hydrogen by deuterium, a slight energetic stabilization was observed, see Figure 3b.

Tautomerization in hypericin is accompanied by reorientation of the S_0–S_1 TDM due to different positions of the carboxyl group, which is exemplarily shown by the colored arrows for the $Q_{7,14}$ and $Q_{1,7}$ tautomer in Figure 3a. Hence, tautomerization can be directly observed by a reorientation of the image patterns, as shown in Figure 1. Comparing the pattern orientation in Figure 1 it is obvious, that the TDM of molecules 3 and 4 show large angle flipping, whereas the pattern orientation of molecules 1, 2, and 5 is quite stable. In the study by Liu et al.,[42] we have shown that for hypericin large-angle variations of the TDM can only be observed if the molecule is nearly perpendicular to the image plane, as there is only a small-angle difference of the

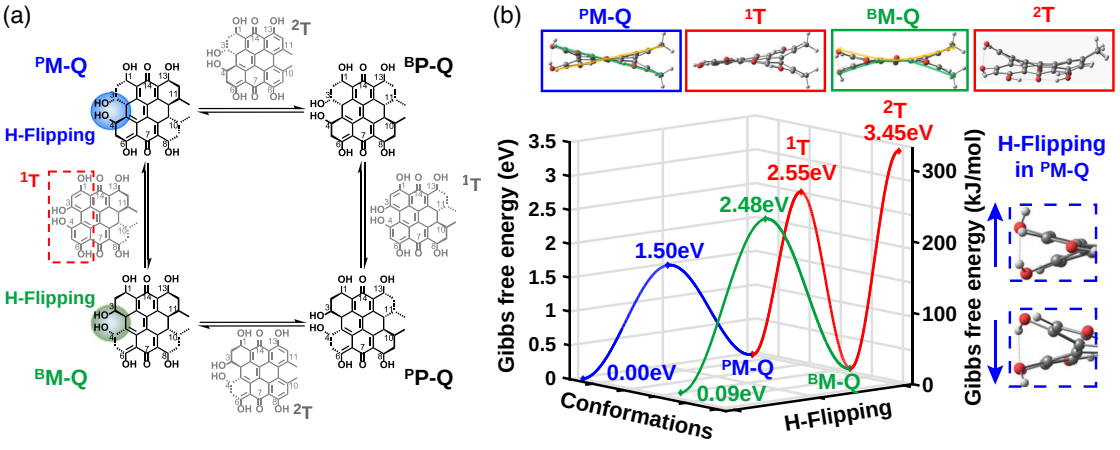

Figure 2. a) Conformational equilibria of the neutral conformers (in black) with the carbonyl group at the positions 7 and 14, and the corresponding transition states (in gray) in the conformational cycle. b) Potential energy curves along the reaction coordinates for the conformational isomerization in red and the H-flip at the bay region of ^{P}M-Q and ^{B}M-Q, as sketched in blue and in green, respectively. The Gibbs free energy of ^{P}M-Q is set as the reference. Inset pictures in squares are ball and stick representations of ^{P}M-Q, ^{B}M-Q, ^{1}T, ^{2}T and H-flipping.

© 2021 The Authors. Advanced Photonics Research published by Wiley-VCH GmbH

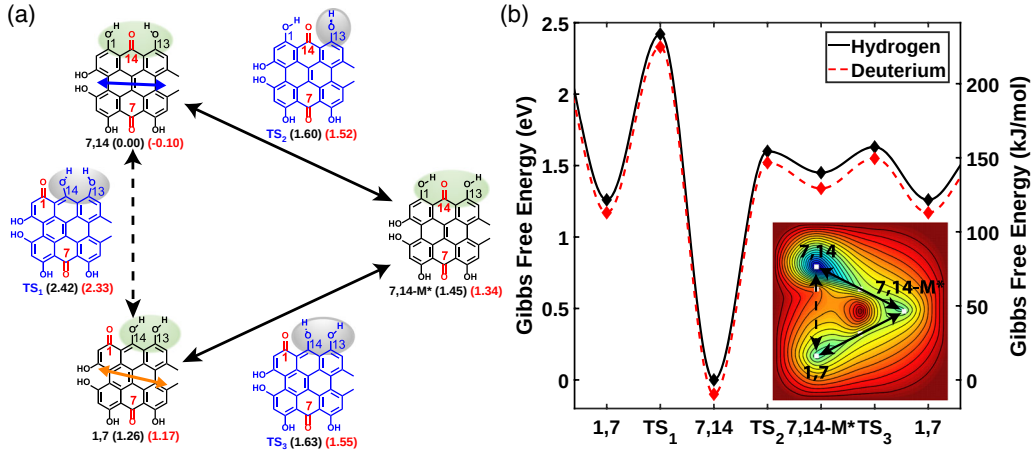

Figure 3. Intramolecular tautomerization between two tautomers, $Q_{7,14}$ and $Q_{1,7}$, in which two carboxyl groups locate at the positions 7,14 and 1,7, with respect to one-proton transfer. a) Schematic representation of two possible pathways in the tautomerization process. Gibbs free energies are labeled in black for neutral hypericin and in red for deuterated hypericin. Colored arrows illustrate the TDM. b) Potential energy curve along the reaction coordinate with a 2D representation of the potential surface.

TDMs of the tautomers (smaller than 24°). Hence, the absence of a flipping pattern does not necessarily mean that there is no tautomerization, but that it is difficult to observe by imaging with the APDM/RPDM. Although, such small-angle variations of the TDM are sometimes hard to be observed in the image patterns, additional information can be extracted from temporal behavior of the fluorescence intensity. **Figure 4** (left column) shows intensity time traces (binning time: 10 ms) of four single hypericin molecules with obvious differences in their temporal emission behavior.

In addition, the intensity autocorrelation function, which reflects fluorescence intensity fluctuation dynamics, can be calculated directly from the time correlated single photon (TCSP) data with a temporal resolution of 64 ps, which is shown in the right column of Figure 4. These autocorrelation functions can be fitted by a stretched exponential function (details are given in Figure S3–6, Supporting Information)

$$g^2(\tau) = G(\tau) - 1 \cong Ae^{-\left(\frac{t}{\tau_1}\right)^{\beta_1}} + Be^{-\left(\frac{t}{\tau_2}\right)^{\beta_2}} \quad (1)$$

The first term with the subscript 1 is used to describe processes in the milliseconds range (blue curves on the right side of Figure 4), whereas the second term is used for dynamics in the seconds range (green curves on the right side of Figure 4). From the fluorescence images in Figure 1, it is already obvious that the blinking dynamics fall into the milliseconds temporal range with a lifetime τ_1 and tautomerization (flipping of the pattern) occurs in the seconds time scale with a tautomerization residence time τ_2, which is the average time a molecule resides in a tautomeric state. Please be aware, that if multiple processes occur within the same temporal window the obtained lifetimes are the mean lifetime of all involved processes. In the following, we will discuss results obtained by fitting of the autocorrelation function of single hypericin molecules illustrating four possible scenarios. The fluorescence emission of the first single hypericin molecule in Figure 4a is comparably stable during the whole acquisition time, until it is photobleached after 77.4 s. The intensity time trace already shows, that there are no apparent intensity fluctuations in the seconds time scale (no tautomerization) and short time scale dynamics are shorter than the binning time of 10 ms. However, the autocorrelation function is directly based on the TCSP counting data with a temporal resolution of 64 ps and allows to determine a lifetime of approximately $\tau_1 \approx 0.01$ ms, which is in the range of triplet state lifetimes of hypericin reported at ambient conditions.[65,66] The lack of long time scale intensity fluctuations is accounted for by $\tau_2 \approx \infty$. The second molecule in Figure 4c shows fast intermittency (blinking) of the fluorescence emission during the whole acquisition time. The corresponding intensity autocorrelation function in Figure 4d is dominated by a single exponential decay with $\tau_1 = 5.9$ ms, which is much longer than the triplet state lifetime shown in Figure 4b. However, such a triplet state lifetime is in agreement with values reported at low temperatures.[35,36] Indeed, embedding hypericin in a 80 nm poly (vinyl alcohol) (PVA) film drastically increases the triplet state lifetime to an average value of $\tau_1 = (6.9 \pm 1.0)$ ms compared with $\tau_1 \approx (0.1 \pm 0.1)$ ms on a glass substrate (see Figure S7a, Supporting Information). This indicates that triplet state of hypericin is less quenched inside a PVA film, possibly due to a reduced amount of oxygen, which plays a major role in quenching of the triplet state.[65–67] In general, the triplet state lifetime of hypericin can be strongly quenched by energy acceptors, electron donors, and acceptor[68,69] and the PVA layer seems to efficiently protect the single hypericin molecules from their influence. Again, $\tau_2 \approx \infty$ in Figure 4d shows that there are no apparent long time scale dynamics. The third hypericin molecule in Figure 4e is an example where multiple fluorescence intensity levels can be observed. These abrupt fluorescence intensity changes can be assigned to tautomerization, since each tautomer has a different spatial orientation of the TDM (see flipping in Figure 1). In general, the excitation rate γ_{exc} is proportional to the absolute square of the scalar product of the TDM and the electric excitation field ($\gamma_{exc} \propto |\vec{P} \cdot \vec{E}|^2$). Hence, reorientation of

© 2021 The Authors. Advanced Photonics Research published by Wiley-VCH GmbH

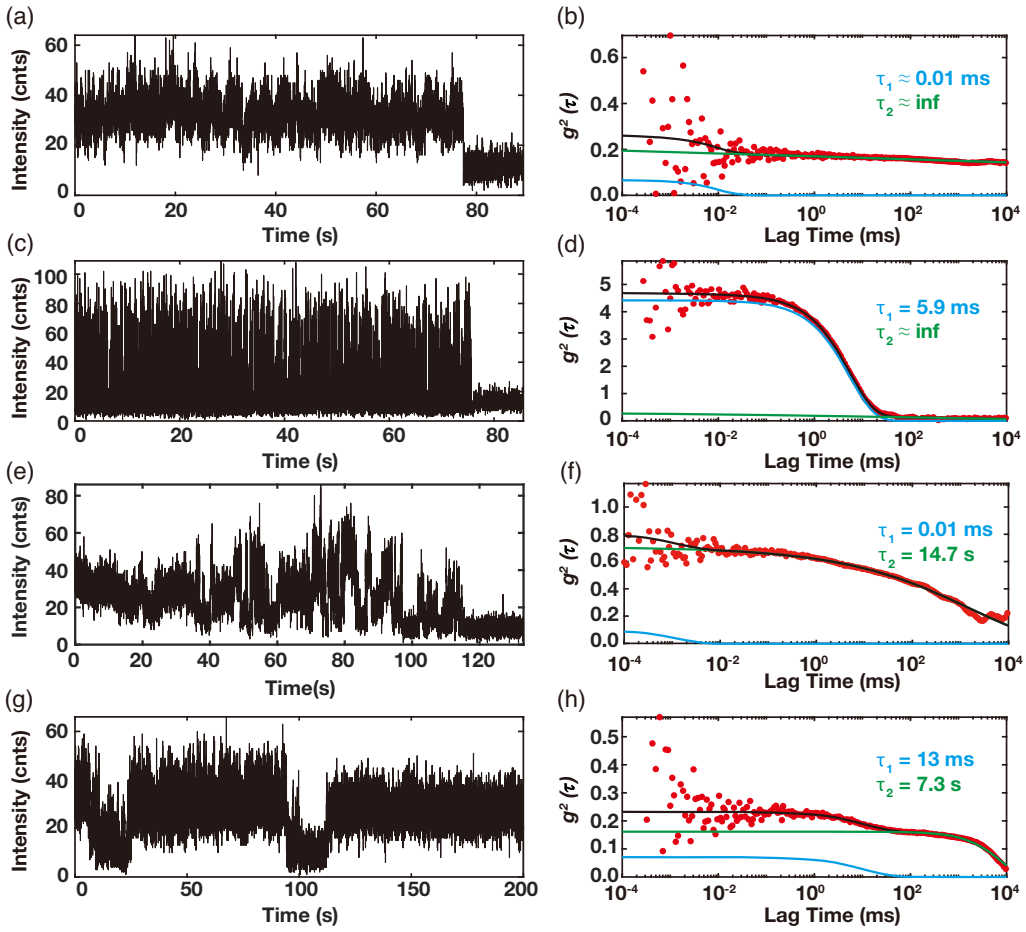

Figure 4. Four intensity time traces of single hypericin molecules and corresponding intensity autocorrelation functions. The first molecule in a,b) does only show very fast ($\tau_1 \approx 0.01$ ms) dynamics and there are no intensity fluctuations on a longer time scale ($\tau_2 \approx$ inf). The intensity time trace of the second molecule in c) is dominated by fast blinking and the autocorrelation function in d) is a single exponential decay with $\tau_1 = 5.9$ ms. The third molecule in e) exhibits large intensity fluctuations in the seconds time scale, which is clearly revealed in f) with a stretched exponential decay with $\tau_2 = 14.7$ s. The molecule in g) is a perfect example showing both short-time blinking ($\tau_1 = 13$ ms) and long-time fluctuations ($\tau_2 = 7.3$ s).

the TDM leads, for a fixed electric field orientation, to a change of the excitation rate for each tautomer, resulting in multiple fluorescence intensity levels. These multiple fluorescence intensity levels suggest, that this hypericin molecule cycles between different tautomeric species in the same temporal window leading to a long exponential decay ($\tau_2 = 14.7$ s) in the autocorrelation function in Figure 4f. The fourth molecule in Figure 4g shows a perfect example showing short (blinking) and long (tautomerization) time scale fluctuations. As expected, the autocorrelation curve in Figure 4h shows a mixture of two exponential decays with $\tau_1 = 13$ ms and $\tau_2 = 7.3$ s. Additional information can be obtained from the stretch parameter $\beta_{1/2}$, which enables to draw conclusions on how many processes are occurring in the corresponding time window. In the following, we want to discuss the meaning of the stretch parameter on the basis of the long term intensity fluctuations, as different scenarios can be intuitively compared with time traces on the left side of Figure 4. The first example is the molecule shown in Figure 4a,b, where no long time scale intensity fluctuation can be observed and fitting the autocorrelation function yields β_2 close to zero, which means that no intensity fluctuations in the seconds time scale are observed during the acquisition time. The second scenario is shown in Figure 4g,h and there are long-term intensity fluctuations between the same intensity levels, i.e., transitions between the same tautomeric species. This single process gives an autocorrelation function, which can be fitted by a single exponential decay giving $\beta_2 = 1$. The third scenario is shown in Figure 4e,f, where the single molecule cycles between different tautomeric species and multiple intensity levels can be observed in the intensity time trace. Such a behavior involving multiple process within the same temporal acquisition yields $\beta_2 = 0.3$ and the tautomerization residence time $\tau_2 = 14.7$ s is the average of all involved processes. The ratio of the amplitudes A, B is a measure if the short or long time scale intensity fluctuations are dominating the temporal emission behavior and, for most cases, we find that triplet blinking dynamics have the strongest influence.

In the following, we will mainly focus on the tautomerization residence time τ_2 obtained from the temporal emission behavior. Nevertheless, all other parameters obtained by fitting the autocorrelation functions are presented in Figure S7, Supporting

© 2021 The Authors. Advanced Photonics Research published by Wiley-VCH GmbH

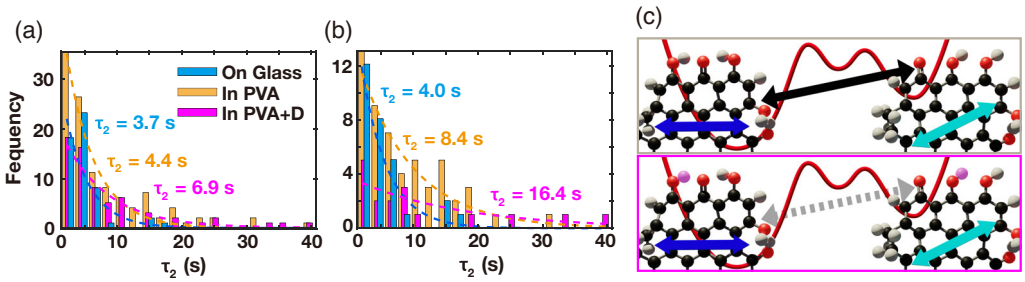

Figure 5. a) Histograms of the tautomerization residence times τ_2 for hypericin on a glass substrate (blue) and for normal (yellow) and deuterated (pink) hypericin embedded in a PVA matrix. The histogram distributions are fitted by an exponential function $y = Ae^{-b\tau}$ giving average tautomerization residence times $\langle\tau_2\rangle = 3.7$ and 4.4 s for hypericin on glass and in PVA. The average tautomerization residence time increases to $\langle\tau_2\rangle = 6.9$ s when hypericin is deuterated, respectively. b) Subpopulation of a) showing molecules with apparent tautomerization. c) Illustration of the reduced tunneling probability by replacing hydrogen with deuterium.

Information. In **Figure 5**a, experimental tautomerization residence times τ_2 are shown for three cases: 1. hypericin directly deposited on a glass substrate (blue), 2. normal (yellow), and 3. deuterated (pink) hypericin embedded in an 80 nm PVA film.

The histograms in Figure 5a are based on $n = 78$, 189, and 89 single hypericin molecules, respectively. The energy barriers between the tautomeric species are larger than the available thermal energy and tautomerization is based on tunneling of a proton. Hence, the tautomerization residence times are expected to follow a Poisson distribution and the histogram distributions can be fitted by an exponentially decaying function $y = Ae^{-b\tau}$ (dashed lines in Figure 5a).[70,71] This yields an average tautomerization residence time of $\langle\tau_2\rangle = 3.7$ s for hypericin on a glass substrate (blue) and $\langle\tau_2\rangle = 4.4$ s inside the PVA film (yellow). However, photo bleaching of the molecule during the acquisition does have an impact on the autocorrelation function, as it drops to zero for lag times larger than the finite survival time T. In the study by Liu et al.,[41] we have determined average survival times of single hypericin molecules of $T = 23.8$ s on glass and $T = 46.6$ s in PVA. These average survival times can be used to exclude molecules where the only "long time scale dynamic" is photo bleaching by considering time traces with tautomerization residence times smaller than the average survival time ($\tau_2 < T$). In addition, single molecules exhibiting multilevel intensity fluctuations do not result in a monoexponential decay of the autocorrelation function ($\beta_2 \neq 1$). Hence, $\tau_2 < T$ and $\beta_2 \neq 1$ are suitable criteria to select intensity time traces with clear tautomerization, one example is shown in Figure 4e. However, this criteria might be even too strict, as single molecules, which are cycling between similar intensity levels (Figure 4g) are also rejected. Nevertheless, this criteria allow to determine the subpopulation of single hypericin molecules showing apparent tautomerization, which is presented in Figure 5b. Here, the average tautomerization residence time is $\langle\tau_2\rangle = 4.0$ s for hypericin on a glass substrate, which increases to $\langle\tau_2\rangle = 8.4$ s in PVA, clearly showing that the embedding matrix influences tautomerization. Tautomerization in hypericin is based on tunneling of a proton, hence a strong dependence on the mass of the tunneling particle is expected and exchanging the tunneling proton with deuterium should result in a significant increase in the tautomerization residence times τ_2. This is shown for deuterated hypericin in pink in Figure 5a,b and the average tautomerization residence time $\langle\tau_2\rangle$ increases from 4.4 to 6.9 s considering the whole dataset, whereas the effect is even more dramatic for the subpopulation showing clear tautomerization in Figure 5b with an increase in $\langle\tau_2\rangle$ from 8.4 to 16.4 s. This proves that the long time scale intensity fluctuations are indeed caused by tunneling of a proton and can be unambiguously attributed to tautomerization, which is schematically shown in Figure 5c.

An interesting approach to alter the optical properties of a single molecule, without changing its chemical structure, is to influence its photonic environment by a $\lambda/2$ wavelength Fabry–Pérot microcavity. Single hypericin molecules are embedded in a thin PVA layer between the two silver mirrors forming the microcavity, which has an optical path length supporting resonances in the visible spectral range. Such a microcavity allows to influence the spontaneous emission rate by the Purcell effect.[57,72,73] A schematic drawing of the microcavity is shown in **Figure 6**a and details are given in the Experimental Section.

In Figure 6, average tautomerization residence times obtained from single hypericin molecules ($n = 189$) embedded in a thin PVA layer outside of the microcavity (free space) are presented in yellow and are compared with results obtain for a microcavity being on- (red, $\lambda_{max} = 613$ nm, $n = 142$) or off-resonance (purple, $\lambda_{max} = 712$ nm, $n = 139$) with the emission maximum ($\lambda_{max} = 603$ nm) of hypericin (see Figure S8, Supporting Information). Again, we want to focus on the tautomerization residence times τ_2, but all other parameters are given in Figure S9, Supporting Information. Nevertheless, it is worth to mention that the triplet state lifetimes in Figure S9a, Supporting Information, are not influenced by the confined optical field in the microcavity and are practically the same for all three cases ($\langle\tau_1\rangle = 7.5$, 7.1, and 7.1 ms, respectively). Interestingly, the long time scale dynamics in Figure 6b show that tautomerization can be influenced by the confined optical field in the microcavity. The average tautomerization residence time $\langle\tau_2\rangle$ decreases from 4.4 s in free space to 2.7 s in the on-resonance microcavity, whereas it slightly increases to 4.7 s in the off-resonance case. Again, this effect is even more dramatic in Figure 6c when only the subpopulation of molecules showing apparent tautomerization is considered. Here, the average tautomerization residence times $\langle\tau_2\rangle$ decreases from 8.4 to 1.4 s in the resonant case and increases to 8.5 s in the off-resonant case. A possible explanation for this decrease in the tautomerization residence time is an altered population of excited vibrational

© 2021 The Authors. Advanced Photonics Research published by Wiley-VCH GmbH

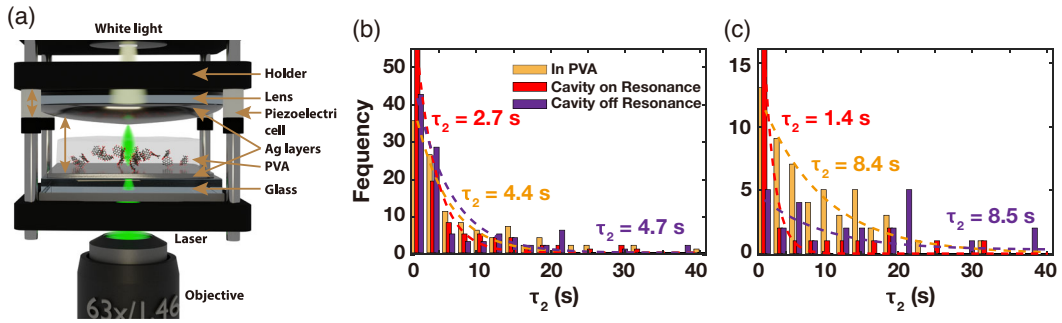

Figure 6. a) Schematic drawing of a $\lambda/2$ microcavity where single hypericin molecules in a PVA layer are positioned between two silver mirrors. Transmission spectra to determine the cavity resonance can be obtained with a white light emitting diode, whereas fluorescence spectra are acquired by focusing a laser beam from below. b) Tautomerization residence time τ_2 obtained from the whole data set giving $\langle\tau_2\rangle = 4.4$, 2.7, and 4.7 s for free space (yellow), on-resonance (red) and off-resonance microcavity (purple), respectively. c) Subpopulation of molecules with multiple tautomerization transitions giving $\langle\tau_2\rangle = 8.4$, 1.4, and 8.5 s.

states by Raman scattering, which has been reported for surface-enhanced Raman scattering even for low excitation powers.[61] Similar nonthermal vibrational populations have been observed on the single molecule level and are explained by a quantum mechanical description,[59,74] where the occupation of vibrational modes (ω_ν), which are on resonance with the detuning ($\Delta \approx \omega_\nu$), are amplified when excitation laser (ω_L) frequency is larger than the cavity resonance frequency ($\Delta = \omega_L - \omega_c > 0$). Here, we have a similar situation where the excitation laser $\lambda_L = 530$ nm is blue shifted to the on-resonance cavity mode at $\lambda_c = 613$ nm, which corresponds to a Raman shift of $\approx 2550\,\mathrm{cm}^{-1}$ and is suitable to influence the pronounced Raman active modes of hypericin between 1200 and 1700 cm^{-1}.[41] The possible nonthermal vibrational distribution caused by the Raman effect can increase thermally activated tautomerization, similar to tautomerization in porphycene,[16] leading to the decreased tautomerization residence time of hypericin in Figure 6. However, tuning the cavity resonance to $\lambda_c = 712$ nm corresonds to a Raman shift of $\approx 4850\,\mathrm{cm}^{-1}$ where the amplification of the Raman modes vanishes due to the large detuning.

3. Conclusion

In this work, we present a comprehensive investigation of the structural dynamics present in hypericin. TD-DFT calculations show that the energy barriers for conformational transitions are significantly larger than values obtained by FF calculations. The energy barriers calculated by FF are 28.3 kJ mol^{-1} (^{1}T state) and 113.4 kJ mol^{-1} (^{2}T state),[27] whereas TD-DFT calculations show that the barriers are significantly higher, giving values of 246 kJ mol^{-1} for the ^{1}T state and 333 kJ mol^{-1} for the ^{2}T state. These high energy barriers yield small tunneling probabilities, which make it unlikely to observe conformational transitions under normal experimental conditions. In addition, we identify a new conformational mechanism in hypericin, which we call H-flipping. Here, the *bay* hydroxyl groups alternatively participate in the formation of the intramolecular hydrogen bond, which is either pointing upward or downward, leading to energy barriers of 145 kJ mol^{-1} in the propeller (^{P}M-Q) and 239 kJ mol^{-1} in the butterfly (^{B}M-Q) conformer. However, such a transition does not change the orientation of the TDM and hence cannot be observed in the optical experiments presented here. However, in Figure 1, we find a spatial reorientation of the TDM and corresponding dynamics can also be observed in the temporal fluorescence emission dynamics in Figure 4. These dynamics cannot be explained by conformational transitions, but are caused by tautomerization. Our TD-DFT calculations show that, in agreement with literature,[26,27] the most stable tautomer of hypericin is the one with the carboxyl groups at position 7,14 and that tautomerization occurs in a two-step process with an intermediate state $Q_{7,14\text{-}M^*}$ (Figure 3). Hence, tautomerization is based on two consecutive vibrationally assisted tunneling processes and replacing the tunneling proton by deuterium leads to a significant reduction of the tautomerization residence time by a factor of 1.95 (Figure 5b). In addition, we find a strong influence of the embedding matrix on the tautomerization rate in Figure 5b and on the triplet state lifetime in Figure S7, Supporting Information, which shows that the local environment has a strong impact on the properties of hypericin. Hence, it is crucial to tailor the environment in, e.g., drug delivery systems for a successful medical application.[75,76] In addition, we show tautomerization can be controlled by the photonic environment in a $\lambda/2$ Fabry–Pérot microcavity, where tautomerization gets faster/slower when the cavity is on/off resonance to the fluorescence emission maximum.

4. Experimental Section

Single-Molecule Spectroscopy: For the single-molecule experiments, hypericin was dissolved in ethanol (Uvasol, Merck) and diluted to a concentration of 10^{-6} M. About 2 µL of the hypericin solution were added to 2 mL of a 2 wt% PVA (Sigma-Aldrich) solution in triply distilled water to achieve a final hypericin concentration of 10^{-9} M. For the deuterium experiments, ethanol was replaced by deuterated methanol-d4 (99% atom D, Sigma-Aldrich) and PVA was dissolved in D_2O (99% atom D, Sigma-Aldrich). These solutions were spin coated on a cleaned glass coverslip to obtain a thin hypericin/PVA film of ≈80 nm thickness. This procedure yields a PVA film with spatially isolated single hypericin molecules (see Figure S10, Supporting Information) with distances larger than the diffraction limited focus of the confocal microscope. For single molecule experiments with hypericin directly deposited on glass, 2 µL of a 10^{-10} M solution was dried on a cleaned coverslip. Fluorescence images of single hypericin molecules were recorded with a home-built scanning confocal

© 2021 The Authors. Advanced Photonics Research published by Wiley-VCH GmbH

microscope (see Figure S11, Supporting Information) with a 530 nm pulsed excitation laser (pulse duration $<$ 100 ps, 20 MHz). A commercial mode converter (polarization converter, Arcoptix) was used to generate the APDM and RPDM for fluorescence images. Linear polarization was used for intensity time traces. A high numerical aperture oil objective lens (NA = 1.46, Carl Zeiss) was used to focus the excitation beam (1.2 μW in front of the objective) on the sample and to collect the fluorescence signal. The sample, either a thin PVA film on glass or a microcavity, was mounted on a scanning piezo-stage (P-527.3CL, Physics Instruments) to acquire images and to address individual molecules. The excitation laser was removed from the detected signal by the 532 nm long pass filter (532LP Edge Basic, Semrock), which was focused on two avalanche photodiodes (APDs, SPCM-AQR-14, PerkinElmer). The APDs were connected to a TCSP counting module (HydraHarp 400, PicoQuant) synchronized with the TTL signal generated by the pulsed laser. A TTL pulse is output from APD and recorded at HydraHarp 400 for each detected photon and saved as a Time-Tagged Time-Resolved file.[77] The autocorrelation function was calculated with recorded files using Symphotime 64 (PicoQuant), and the fitting of the autocorrelation function was achieved using a self-written Matlab scripts.

Microcavity: For the microcavity experiments, a flat and a curved mirror were assembled in a home-built holder to form the microcavity (schematic drawing in Figure 6a), which had a quality factor of roughly 20. The flat mirror consisted of a 1 nm chromium, 30 nm silver, and 50 nm silica layer evaporated on a cleaned glass coverslip. The curved mirror was prepared by evaporating 1 nm chromium, 50 nm silver, and 50 nm silica on a planoconvex lens (Thorlabs, f = 50 mm). Here, chromium acted as an adhesion layer, and the silica layer protected the mirror from oxidation and mechanical damage. In addition, the silica layer served as a spacer layer to avoid quenching by the silver mirror. Similar to the free space experiment, a thin hypericin/PVA film was spin coated on top of the flat mirror and the silica spacer layer allowed to position the film roughly in the center of the microcavity. The microcavity resonance could be determined by acquiring the white light transmission spectrum (see Figure S8, Supporting Information) and was set to 613 nm/712 nm for on/off-resonance measurements by approaching the curved mirror toward the flat mirror by a piezoactuator (Thorlabs Polaris Kinematic Mirror Mounts KC1-T-PZ). Because the cavity strongly reflected the laser, the excitation laser power was increased to 4 μW in front of the objective to ensure that the fluorescence signal can be detected. The average reflectivities, calculated using Transfer Matrix Method,[78] were 92.7% for cavity on resonance and 94.3% for cavity off resonance, which corresponded to the excitation power of 0.29 and 0.23 μW, respectively.

DFT and TD-DFT Calculations: The electronic ground and transition state optimizations on the full structure of hypericin were carried out by DFT calculations without any symmetry restrictions to model molecules in vacuum. TDM orientations were calculated by TD-DFT. For all cases, the B3LYP functional[79] and the 6–311G* basis set were used as implemented in the Gaussian 16 program package. TDM orientations should be little affected by this. As this work focused on the stereochemical complexity of hypericin, i.e., the conformational and tautomeric dynamics, four conformational isomers of the most stable tautomer $Q_{7,14}$, namely ^{P}M-Q, ^{B}M-Q, and their enantiomeric pairs ^{P}P-Q, ^{B}P-Q, as well as ten tautomers of the most stable conformer ^{P}M-Q were identified. Relative stabilities of conformational isomers were investigated earlier by ab initio FF[27,64] and restricted Hartree–Fock (HF) calculations[28] as well as by DFT.[80] In addition, the tautomers of hypericin were calculated by FF,[27,64,81] semiempirical AM1,[29] and restricted HF[28] calculations; however, a systematic study at the DFT level had not been reported so far. Conformers were achieved by torsions of the aromatic backbone, characterized by two dihedral angles $\Theta_{3,3a,4a,4}$ and $\Theta_{10,10a,11a,11}$, whereas tautomers are defined by the positions of the carboxyl groups at the *peri* region. All energy minima were confirmed by the absence of imaginary frequencies. Furthermore, transitions states in the conformational isomerization, tautomerization, and the newly defined H-flip at the 3-, 4-position were studied in detail. The transition states were characterized by one imaginary frequency, referring to a local maximum (the saddle point), and reflecting the dynamic pathway between two adjacent local minima.[82]

Supporting Information

Supporting Information is available from the Wiley Online Library or from the author.

Acknowledgements

Q.L. and L.W. contributed equally to this work. The authors gratefully acknowledge funding by the German Research Foundation (DFG, ME 1600/13-3) and the Funding of China Scholarship Council (CSC). The work in Madrid was supported by the Spanish Science Ministry (MINECO-FEDER projects CTQ2017-87054, SEV-2016-0686) and by the Campus of International Excellence (CEI) UAM+CSIC. L.W. acknowledges an Erasmus+ grant of the European Commission. L.W. and J.G. thank Begoña Milián-Medina, Valencia for discussion.

Conflict of Interest

The authors declare no conflict of interest.

Data Availability Statement

Research data are not shared.

Keywords

hypericin, intensity autocorrelation, single molecule microscopy, tautomerization, time-dependent density functional theory, tunneling

Received: December 2, 2020
Revised: February 12, 2021
Published online:

[1] O. K. Abou-Zied, R. Jimenez, F. E. Romesberg, *J. Am. Chem. Soc.* **2001**, *123*, 4613.
[2] T. ten Brink, T. E. Exner, *J. Chem. Inf. Model* **2009**, *49*, 1535.
[3] M. Liu, M. Yuan, M. Luo, X. Bu, H.-B. Luo, X. Hu, *Biophys. Chem.* **2010**, *147*, 28.
[4] S. Natesan, R. Subramaniam, C. Bergeron, S. Balaz, *J. Med. Chem.* **2012**, *55*, 2035.
[5] C. de Oliveira, H. S. Yu, W. Chen, R. Abel, L. Wang, *J. Chem. Theory Comput.* **2019**, *15*, 424.
[6] P. Pospisil, P. Ballmer, L. Scapozza, G. Folkers, *J. Recept. Signal Transduct.* **2003**, *23*, 361.
[7] H. A. Duarte, S. Carvalho, E. B. Paniago, A. M. Simas, *J. Pharm. Sci.* **1999**, *88*, 111.
[8] Y. C. Martin, *J. Comput. Aided Mol. Des.* **2009**, *23*, 693.
[9] P. J. Taylor, G. van der Zwan, L. Antonov, *Tautomerism: methods and theories* **2014**, 1.
[10] D. K. Maity, T. N. Truong, *J. Porphyrins Phthalocyanines* **2001**, *05*, 289.
[11] J. Braun, M. Koecher, M. Schlabach, B. Wehrle, H.-H. Limbach, E. Vogel, *J. Am. Chem. Soc.* **1994**, *116*, 6593.
[12] H.-H. Limbach, J. M. Lopez, A. Kohen, *Philos. Trans. R. Soc. B* **2006**, *361*, 1399.
[13] J. Waluk, *Chem. Rev.* **2017**, *117*, 2447.
[14] M. Koch, M. Pagan, M. Persson, S. Gawinkowski, J. Waluk, T. Kumagai, *J. Am. Chem. Soc.* **2017**, *139*, 12681.
[15] P. Ciąćka, P. Fita, A. Listkowski, C. Radzewicz, J. Waluk, *J. Phys. Chem. Lett.* **2016**, *7*, 283.
[16] Y. Litman, J. O. Richardson, T. Kumagai, M. Rossi, *J. Am. Chem. Soc.* **2019**, *141*, 2526.

© 2021 The Authors. Advanced Photonics Research published by Wiley-VCH GmbH

[17] J. Braun, H.-H. Limbach, P. G. Williams, H. Morimoto, D. E. Wemmer, *J. Am. Chem. Soc.* **1996**, *118*, 7231.
[18] R. M. Dickson, D. J. Norris, Y.-L. Tzeng, W. Moerner, *Science* **1996**, *274*, 966.
[19] H. P. Lu, X. S. Xie, *Nature* **1997**, *385*, 143.
[20] M. Brecht, H. Studier, V. Radics, J. B. Nieder, R. Bittl, *J. Am. Chem. Soc.* **2008**, *130*, 17487.
[21] L. Piatkowski, C. Schanbacher, F. Wackenhut, A. Jamrozik, A. J. Meixner, J. Waluk, *J. Phys. Chem. Lett.* **2018**, *9*, 1211.
[22] A. Kubin, F. Wierrani, U. Burner, G. Alth, W. Grunberger, *Curr. Pharm. Des.* **2005**, *11*, 233.
[23] P. Agostinis, A. Vantieghem, W. Merlevede, P. A. M. de Witte, *Int. J. Biochem. Cell Biol.* **2002**, *34*, 221.
[24] T. A. Theodossiou, J. S. Hothersall, P. A. De Witte, A. Pantos, P. Agostinis, *Mol. Pharm.* **2009**, *6*, 1775.
[25] R. Ritz, M. Müller, M. Weller, K. Dietz, S. Kuci, F. Roser, M. Tatagiba, *Int. J. Oncol.* **2005**, *27*, 1543.
[26] H. Falk, *Angew. Chem. Int. Ed.* **1999**, *38*, 3116.
[27] C. Etzlstorfer, H. Falk, N. Müller, W. Schmitzberger, U. G. Wagner, *Monatsh. Chem.* **1993**, *124*, 751.
[28] J. W. Petrich, M. S. Gordon, M. Cagle, *J. Phys. Chem. A* **1998**, *102*, 1647.
[29] I. Gutman, Z. Marković, S. Solujić, S. Sukdolak, *Monatsh. Chem.* **1998**, *129*, 481.
[30] J. Petrich, *Int. Rev. Phys. Chem.* **2000**, *19*, 479.
[31] D. S. English, W. Zhang, G. A. Kraus, J. W. Petrich, *J. Am. Chem. Soc.* **1997**, *119*, 2980.
[32] K. Das, E. Dertz, J. Paterson, W. Zhang, G. A. Kraus, J. W. Petrich, *J. Phys. Chem. B* **1998**, *102*, 1479.
[33] K. Das, A. V. Smirnov, M. D. Snyder, J. W. Petrich, *J. Phys. Chem. B* **1998**, *102*, 6098.
[34] J. L. Wynn, T. M. Cotton, *J. Phys. Chem.* **1995**, *99*, 4317.
[35] A. Angerhofer, H. Falk, J. Meyer, G. Schoppel, *J. Photoch. Photobio. B* **1993**, *20*, 133.
[36] S. M. Arabei, J. P. Galaup, P. Jardon, *Chem. Phys. Lett.* **1997**, *270*, 31.
[37] T. Yamazaki, N. Ohta, I. Yamazaki, P. S. Song, *J. Phys. Chem.* **1993**, *97*, 7870.
[38] D. Jancura, S. Sánchez-cortés, E. Kocisova, A. Tinti, P. Miskovsky, A. Bertoluzza, *Biospectroscopy* **1995**, *1*, 265.
[39] G. Lajos, D. Jancura, P. Miskovsky, J. V. García-Ramos, S. Sanchez-Cortes, *J. Phys. Chem. C* **2008**, *112*, 12974.
[40] L. N. Raser, S. V. Kolaczkowski, T. M. Cotton, *Photochem. Photobiol.* **1992**, *56*, 157.
[41] Q. Liu, F. Wackenhut, O. Hauler, M. Scholz, S. zur Oven-Krockhaus, R. Ritz, P.-M. Adam, M. Brecht, A. J. Meixner, *J. Phys. Chem. A* **2020**, *124*, 2497.
[42] Q. Liu, F. Wackenhut, L. Wang, O. Hauler, J. C. Roldao, P.-M. Adam, M. Brecht, J. Gierschner, A. J. Meixner, *J. Phys. Chem. Lett.* **2021**, 1025.
[43] W. P. Oziminski, A. Wójtowicz, *Struct. Chem.* **2020**, *31*, 657.
[44] L. Simón, J. M. Goodman, *Org. Biomol. Chem.* **2011**, *9*, 689.
[45] J. Gierschner, M. Ehni, H.-J. Egelhaaf, B. Milián Medina, D. Beljonne, H. Benmansour, G. C. Bazan, *J. Chem. Phys.* **2005**, *123*, 144914.
[46] T. Züchner, A. V. Failla, A. J. Meixner, *Angew. Chem. Int. Ed.* **2011**, *50*, 5274.
[47] Q. Zhan, J. Leger, *Opt. Express* **2002**, *10*, 324.
[48] R. Dorn, S. Quabis, G. Leuchs, *Phys. Rev. Lett.* **2003**, *91*, 233901.
[49] A. V. Failla, H. Qian, H. Qian, A. Hartschuh, A. J. Meixner, *Nano Lett.* **2006**, *6*, 1374.
[50] L. Novotny, M. R. Beversluis, K. S. Youngworth, T. G. Brown, *Phys. Rev. Lett.* **2001**, *86*, 5251.
[51] F. Wackenhut, A. V. Failla, T. Züchner, M. Steiner, A. J. Meixner, *Appl. Phys. Lett.* **2012**, *100*, 263102.
[52] M. A. Lieb, J. M. Zavislan, L. Novotny, *J. Opt. Soc. Am. B* **2004**, *21*, 1210.
[53] H. Piwoński, C. Stupperich, A. Hartschuh, J. Sepioł, A. Meixner, J. Waluk, *J. Am. Chem. Soc.* **2005**, *127*, 5302.
[54] E. M. Purcell, *Confined Electrons and Photons*, Springer **1995**, pp. 839–839.
[55] A. Konrad, A.-L. Trost, S. Skandary, M. Hussels, A. J. Meixner, N. V. Karapetyan, M. Brecht, *Phys. Chem. Chem. Phys.* **2014**, *16*, 6175.
[56] H. Kaupp, T. Hümmer, M. Mader, B. Schlederer, J. Benedikter, P. Haeusser, H.-C. Chang, H. Fedder, T. W. Hänsch, D. Hunger, *Phys. Rev. Appl.* **2016**, *6*, 054010.
[57] A. M. Kern, D. Zhang, M. Brecht, A. I. Chizhik, A. V. Failla, F. Wackenhut, A. J. Meixner, *Chem. Soc. Rev.* **2014**, *43*, 1263.
[58] D. O. Bracher, X. Zhang, E. L. Hu, *Proc. Natl. Acad. Sci. U.S.A.* **2017**, *114*, 4060.
[59] T. Neuman, R. Esteban, G. Giedke, M. K. Schmidt, J. Aizpurua, *Phys. Rev. A* **2019**, *100*, 043422.
[60] M. K. Schmidt, R. Esteban, A. González-Tudela, G. Giedke, J. Aizpurua, *ACS Nano* **2016**, *10*, 6291.
[61] K. Kneipp, Y. Wang, H. Kneipp, I. Itzkan, R. R. Dasari, M. S. Feld, *Phys. Rev. Lett.* **1996**, *76*, 2444.
[62] P. Roelli, C. Galland, N. Piro, T. J. Kippenberg, *Nat. Nanotechnol.* **2016**, *11*, 164.
[63] H. Piwoński, A. Hartschuh, N. Urbańska, M. Pietraszkiewicz, J. Sepioł, A. J. Meixner, J. Waluk, *J. Phys. Chem. C* **2009**, *113*, 11514.
[64] C. Etzlstorfer, H. Falk, M. Oberreiter, *Monatsh. Chem.* **1993**, *124*, 923.
[65] S. Datta, A. Hovan, A. Jutková, S. G. Kruglik, D. Jancura, P. Miskovsky, G. Bánó, *J. Phys. Chem. B* **2018**, *122*, 5154.
[66] P. Gbur, , *J. Lumin.* **2008**, *128*, 765.
[67] A. Hovan, S. Datta, S. G. Kruglik, D. Jancura, P. Miskovsky, G. Bánó, *J. Phys. Chem. B* **2018**, *122*, 5147.
[68] A. P. Darmanyan, W. S. Jenks, D. Eloy, P. Jardon, *J. Phys. Chem. B* **1999**, *103*, 3323.
[69] A. Michaeli, A. Regev, Y. Mazur, J. Feitelson, H. Levanon, *J. Phys. Chem.* **1993**, *97*, 9154.
[70] C. Wasshuber, Dissertation, Technische Univ. Wien **1997**.
[71] S. M. Ross, J. J. Kelly, R. J. Sullivan, W. J. Perry, D. Mercer, R. M. Davis, T. D. Washburn, E. V. Sager, J. B. Boyce, V. L. Bristow, *Stochastic processes* Wiley, New York, **1996**, *2*.
[72] A. Chizhik, F. Schleifenbaum, R. Gutbrod, A. Chizhik, D. Khoptyar, A. J. Meixner, J. Enderlein, *Phys. Rev. Lett.* **2009**, *102*, 073002.
[73] S. Bär, A. Chizhik, R. Gutbrod, F. Schleifenbaum, A. Chizhik, A. J. Meixner, *Anal. Bioanal. Chem.* **2010**, *396*, 3.
[74] F. Benz, M. K. Schmidt, A. Dreismann, R. Chikkaraddy, Y. Zhang, A. Demetriadou, C. Carnegie, H. Ohadi, B. de Nijs, R. Esteban, J. Aizpurua, J. J. Baumberg, *Science* **2016**, *354*, 726.
[75] F. A. P. de Morais, R. S. Gonçalves, B. H. Vilsinski, É. L. de Oliveira, N. L. Rocha, N. Hioka, W. Caetano, *J. Photoch. Photobio. B* **2019**, *190*, 118.
[76] F. A. P. de Morais, R. S. Gonçalves, B. H. Vilsinski, D. Lazarin-Bidóia, R. B. Balbinot, T. M. Tsubone, K. Brunaldi, C. Vatatu Nakamura, N. Hioka, W. Caetano, *Photochem. Photobiol. Sci.* **2020**, *19*, 620.
[77] W. Becker, *Advanced Time-Correlated Single Photon Counting Techniques*. Springer Science & Business Media: **2005**, Vol. *81*.
[78] B. Harbecke, *Appl. Phys. B* **1986**, *39*, 165.
[79] (see e.g., B. M. Wong, T. H. Hsieh, *J. Chem. Theory Comput.* **2010**, *6*, 3704–3712), TDM orientations should be little affected by this.
[80] R. C. Guedes, L. A. Eriksson, *J. Photochem. Photobiol. A* **2005**, *172*, 293.
[81] C. Etzlstorfer, H. Falk, *Monatsh. Chem.* **1998**, *129*, 855.
[82] I. Tuñón, I. H. Williams, *Adv. Phys. Org. Chem.* (Eds: I. H. Williams, N. H. Williams) Academic Press, Vol. *53* **2019**, pp. 29–68.

© 2021 The Authors. Advanced Photonics Research published by Wiley-VCH GmbH